Interplay between Charge Order, Ferroelectricity, and Ferroelasticity: Tungsten Bronze Structures as a Playground for Multiferroicity

Kunihiko Yamauchi and Silvia Picozzi
Consiglio Nazionale delle Ricerche (CNR-SPIN), 67100 L'Aquila, Italy

(Received 10 December 2009; published 1 September 2010)

Charge order is proposed as a driving force behind ferroelectricity in iron fluoride $K_{0.6}Fe^{II}_{0.6}Fe^{III}_{0.4}F_3$. By means of density functional theory, we propose several noncentrosymmetric d^5/d^6 charge-ordering patterns, each giving rise to polarization with different direction and magnitude. Accordingly, we introduce the concept of ''ferroelectric anisotropy'' (peculiar to improper ferroelectrics with polarization induced by electronic degrees of freedom), denoting the small energy difference between competing charge-ordered states. Moreover, we suggest a novel type of charge-order-induced ferroelasticity: a monoclinic distortion is induced by a specific charge-ordering pattern, which, in turn, determines the direction of polarization. $K_{0.6}Fe^{II}_{0.6}Fe^{III}_{0.4}F_3$ therefore emerges as a prototypical compound, in which the intimately coupled electronic and structural degrees of freedom result in a peculiar multiferroicity.

DOI: 10.1103/PhysRevLett.105.107202 PACS numbers: 75.85.+t, 62.20.D−, 77.80.Fm, 85.50.Gk

Materials which combine magnetism and ferroelectricity, belonging to the intriguing class of multiferroics, can be classified into two categories [1]: ''structural magnetic ferroelectrics,'' where the primary order parameter in the ferroelectric (FE) phase transition is related to a structural instability (which can be polar or nonpolar; i.e., $BiFeO_3$ or $YMnO_3$), and ''electronic magnetic ferroelectrics,'' where the primary order parameter is related to electronic degrees of freedom, such as spin, charge, or orbital order [2–5].

Whereas plenty of studies focused on spin-driven ferroelectricity, ferroelectricity induced by charge order (CO) still constitutes a largely unexplored territory. Even in the two paradigmatic cases in which the pattern of Fe^{2+} and Fe^{3+} ions was suggested to break space inversion symmetry, e.g., $LuFe_2O_4$ [6] and Fe_3O_4 [7,8], the actual occurrence of ferroelectricity seems controversial.

Within this context, materials other than oxides—and fluorides in particular—are interesting candidates as potentially novel improper multiferroics. Indeed, $K_{0.6}Fe^{II}_{0.6}Fe^{III}_{0.4}F_3$, which crystallizes in a noncentrosymmetric tetragonal tungsten bronze (TTB) structure, has been reported to show CO, although the exact CO pattern is still debated [9]. The family of TTB compounds, obtained by substituting either tungsten with transition metals or oxygen with other anions, exhibit a lot of functionalities, such as ferroelectricity, ferroelasticity, pyro- or piezoelectricity [10]. Despite such a remarkable technological appeal, TTB compounds have not been deeply investigated from the theory point of view, mainly because of the complex crystal structure. Guided by its high potential, we here focus on $K_{0.6}Fe^{II}_{0.6}Fe^{III}_{0.4}F_3$, showing ferroelasticity and ferroelectricity driven by noncentroymmetric Fe-d^5/d^6 CO patterns. To outline the novel physics in $K_{0.6}Fe^{II}_{0.6}Fe^{III}_{0.4}F_3$, we will first discuss the prototypical TTB compound, $Ba_2NaNb_5O_{15}$ (BNN) [11], where ferroelectricity is driven by conventional Nb^{5+} off centering.

Methodology and structural details.—DFT simulations were performed using the VASP code [12] and the projector augmented wave pseudopotentials [13] within the GGA + U formalism [14] ($U = 5$ eV and $J = 0$ eV for Fe d states). The cutoff energy for the plane-wave expansion of the wave function was set to 400 eV and $\mathbf{k}$-point shells of (4, 4, 16) for BNN and (2, 2, 4) for $K_{0.6}Fe^{II}_{0.6}Fe^{III}_{0.4}F_3$ were used for the Brillouin zone integration. The internal atomic coordinates were optimized until the atomic forces were less than 0.01 eV/Å while the lattice parameters were taken from experiments [9,15]. The FE polarization P was calculated using the Berry phase method [16], by comparing the FE and paraelectric state; the latter is constructed by imposing the x, y, z reflection in the atomic structure. For simplicity, $K_{0.6}Fe^{II}_{0.6}Fe^{III}_{0.4}F_3$ was treated as a ferromagnet; further complexity of the experimentally suggested ferri- or weak ferromagnetic spin configuration is not expected to affect CO (and related ferroelectricity), as in $LuFe_2O_4$ [17].

d^0-ness at $Ba_2NaNb_5O_{15}$.—At room temperature, BNN crystallizes in the polar orthorhombic $Cmm2$ structure with $a = 17.626$, $b = 17.592$, $c = 3.995$ Å [15]. At low temperature, BNN shows quasicommensurate and incommensurate phases with *ferroelastic* (FEL) transition, leading to a crystal cell in the ab plane larger than the above mentioned unit cell [18]. Since ferroelectricity was reported not to be coupled with ferroelasticity [19] and since our main focus is on FE properties, we optimized BNN in the $Cmm2$ structure. As shown in Fig. 1, the optimized NbO_6 octahedrons are significantly distorted from the tetragonal symmetry. The polar distortion along the z axis is driven by the off-center shift of Nb atoms, due to a strong hybridization between Nb empty $4d$ and O $2p$ states, with an average Nb^{5+} ionic displacement (with respect to the side O ions) of 0.16 Å. The FE behavior can be clearly interpreted on the basis of the ''d^0-ness'' criterion [20]. The latter does

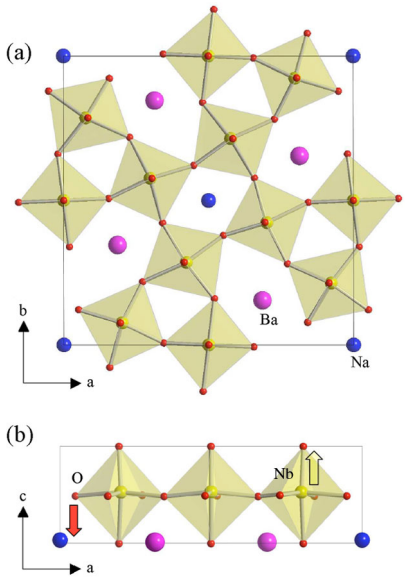

FIG. 1 (color online). C-centered primitive unit cell of the BNN crystal structure in (a) *ab* plane and in (b) *ac* plane (only three Nb-O_6 octahedrons are shown). Upon ionic relaxation, all Nb (O) ions are displaced toward the $+z(-z)$ direction, so as to induce P_z. In $K_{0.6}Fe^{II}_{0.6}Fe^{III}_{0.4}F_3$, the TTB layer is doubled along the *c* axis, where Ba, Na, Nb, and O are replaced by K, K, Fe, and F atoms, respectively.

not only cause electric polarization, but also results in a wide energy gap: 2.29 eV in the FE phase, with respect to 1.75 eV in the paraelectric state. The calculated polarization is $P_z = 34.8\ \mu C/cm^2$; to our best knowledge, this is the first theoretical estimate reported in the literature and is in good agreement with the experimental value of 40 $\mu C/cm^2$ [21].

Charge order at $K_{0.6}Fe^{II}_{0.6}Fe^{III}_{0.4}F_3$.—In iron fluoride, the complexity of the different phase transitions is still a matter of debate. Earlier experiments showed coupled FE/FEL transitions to occur at 490 K [22], along with CO [23]. More recently, several transitions were reported [9]: a first structural transition around 570 K from tetragonal to orthorhombic, a second transition at 490 K where Fe^{2+}/Fe^{3+} CO occurs, and a third transition around 290 K to monoclinic, coupled with ferroelasticity. Experimentally, the orthorhombic *Pba*2 structure was reported, with $a = 12.751$, $b = 12.660$, and $c = 7.975$ Å [9]. From the symmetry point of view, the *Pba*2 group has four symmetry operations: $\{E, C_{2z}, \sigma_x + (\frac{1}{2}\frac{1}{2}0), \sigma_y + (\frac{1}{2}\frac{1}{2}0)\}$ so that FE polarization is, in principle, allowed only along the *z* axis. Given the d^5/d^6 electronic configuration of Fe ions, P_z by "d^0-like" hybridization is of course not expected here, so that alternative mechanisms, such as CO, should be invoked to explain ferroelectricity. As discussed in Ref. [9], the Fe ions in two FeO layers show CO, whose pattern varies with respect to the $K_{0.53}FeF_3$ case (with less K and with the tetragonal structure $P4_2bc$) [24]. However, the CO at $K_{0.6}Fe^{II}_{0.6}Fe^{III}_{0.4}F_3$ is not "full" in the experimental *Pba*2 structure: although 12 Fe ions are supposed to be $Fe^{2+}(d^6)$ and 8 Fe ions to be $Fe^{3+}(d^5)$ due to the stoichiometry ($K_{12}Fe^{II}_{12}Fe^{III}_{8}F_{60}$/cell), the *Pba*2 crystal structure gives 10 Fe^{2+}, 6 Fe^{3+}, and 4 $Fe^{2.5+}$ ions [cf. Figs. 2(a) and 2(b)]. As expected, the mixed-valence Fe ions lead to a metallic behavior (not shown), kept even after the structural optimization. In order to obtain an insulating state (needed for ferroelectricity), the symmetry must be reduced so as to get a fully COed Fe sublattice. Although a larger monoclinic supercell has been previously suggested to explain the twinning satellite observed by electron-diffraction [9], we assume that the CO pattern, determined in the *Pba*2 unit cell, is not affected by expanding the unit cell. This is because such a monoclinic superstructure modulation, typical for BNN structure, mainly consists in tilting the FeF_6 octahedrons, but it does not change the Fe-F bond length [24] so as not to affect the Fe^{2+}/Fe^{3+} pattern. Therefore, we limited our study to the *Pba*2 unit cell [25].

Here we assumed three CO patterns, COI, COII, and COIII, each keeping one of the three symmetry operations and breaking the other two among C_{2z}, $\sigma_x + (\frac{1}{2}\frac{1}{2}0)$, and $\sigma_y + (\frac{1}{2}\frac{1}{2}0)$, respectively, [cf. Fig. 2(c)]. Whereas the induced polarization P_z is allowed by the prototype *Pba*2, P_y and P_x are additionally allowed in COII and COIII, respectively.

After ionic optimization at each CO pattern, the charge separation between Fe^{2+} and Fe^{3+}, calculated by integrat-

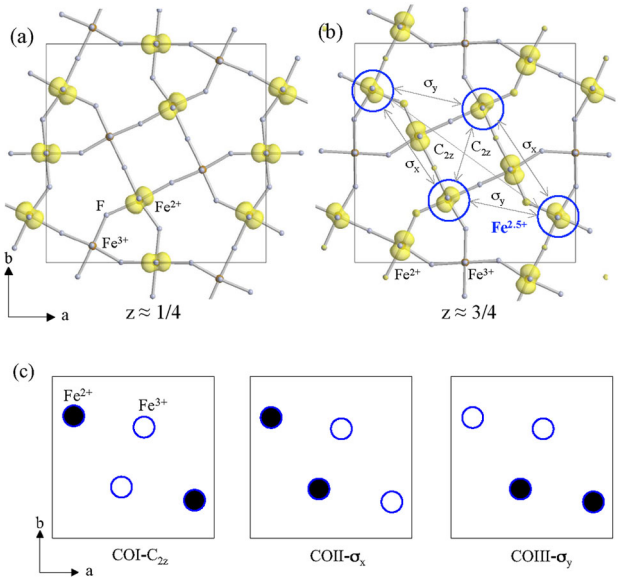

FIG. 2 (color online). Down-spin charge of Fe t_{2g} state, 1 eV below E_F, for the *Pba*2 symmetry at (a) $z \approx 1/4$ and (b) $z \approx 3/4$ planes. Circled ions are mixed-valence $Fe^{2.5+}$ ions. The symmetry operations which relate the four $Fe^{2.5+}$ are also shown. (c) Full CO patterns starting from partial CO shown in (b) can be obtained by turning four $Fe^{2.5+}$ sites into two Fe^{2+} and two Fe^{3+} sites at $z \approx 3/4$ plane. The positions of [open (blue)] circles correspond to the circles in (b).

TABLE I. Total energy difference (meV/Fe), energy gap (eV), and induced FE polarization calculated by Berry phase P^{Berry}, by dipoles P^{dipole}, and by point-charge model P^{PCM} (μC/cm^2) at partial CO pattern in experimental crystal structure (Exp), optimized structure keeping experimental symmetry (Opt), full CO patterns; COI, COII, COIII (with given symmetry).

	Exp	Opt	COI-C_{2z}	COII-σ_x	COIII-σ_y
	$Pba2$	$Pba2$	$P2$	Pc	Pc
ΔE^{tot}	0	−31.3	−44.3	−57.3	−51.6
E^{gap}	0	0	0.91	1.28	1.08
P^{Berry}	–	–	(0 0 0.09)	(0 −0.50 −0.19)	(−5.14 0 0.03)
P^{dipole}	–	–	–	$P_y = -0.57$	$P_x = -5.43$
P^{PCM}	–	–	–	$P_y = -0.49$	$P_x = -5.40$

ing the charge density in 1 Å atomic radius, is equal to $0.365e^-$; rather large compared to Fe_3O_4 ($\approx 0.2e^-$) [8]. Indeed, this is consistent with the expected weaker Fe-F hybridization compared to Fe-O and put forward fluorides as better candidates for CO—compared to oxides—where a larger charge-disproportionation can be achieved.

CO-induced ferroelectricity.—We found that among the assumed CO patterns as well as the experimental or optimized state, COII is the most stable state with the largest energy gap [cf. Table I]. Besides, COII shows a sizeable polarization $P_y^{\text{Berry}} = -0.50\ \mu\text{C/cm}^2$. This can be roughly understood as induced by local electric "point-charge" dipoles which connect Fe^{2+} and Fe^{3+} ions, as suggested for Fe_3O_4 [8,25]. The electric dipoles are calculated considering only four Fe ions, i.e., those originally located on the mixed valence sites. In fact, the CO pattern of the other Fe ions is identical to the high-symmetry $Pba2$ CO, so that their net contribution to **P** would cancel out. As shown in Figs. 3(b) and 3(c), P_y^{dipole} is calculated as $-0.57\ \mu\text{C/cm}^2$, in good agreement both with P_y^{Berry} and P_y^{PCM} (taking into account all the ions with their nominal valencies): this shows that polarization has a purely electronic origin and that ionic displacements play a minor role. Note that the sign of P_y can be switched by exchanging Fe^{2+} and Fe^{3+} ions; under an applied electric field E_y, charge shifts among these four Fe sites is indeed expected to occur. In an analogous way, we calculated P_x at the COIII pattern as $P_x^{\text{dipole}} \simeq P_x^{\text{Berry}} \simeq P_x^{\text{PCM}} \simeq -5\ \mu\text{C/cm}^2$, a value much larger than P at COII. In this case, too, the agreement between P_x^{dipole} and P_x^{Berry} is remarkable. Finally, as expected, the CO-induced polarization, though sizeable, is much smaller than in BNN where ionic degrees of freedom are the source of ferroelectricity.

Charge and orbital order.—The CO arrangement also causes a change in the Fe-t_{2g}^1 orbital ordering (OO). When comparing Figs. 2 and 3, the occupied t_{2g} orbitals modify their shape or direction to avoid as much as possible the nearest t_{2g}-t_{2g} overlap. Figure 4 shows the three-dimensional network of Fe-t_{2g} OO. Clearly the t_{2g}-orbital relative to the "extra charge" on the Fe^{2+} site at COII is aligned along a diagonal direction in the octahedron. This both reduces the strong intersite Coulomb interaction with neighboring t_{2g}-orbitals at Fe^{2+} sites and optimizes the cooperative Jahn-Teller distortion, making COII energetically lower than COIII.

CO-induced ferroelasticity.—From the above discussions, we conclude that the ground state of $K_{0.6}Fe^{II}_{0.6}Fe^{III}_{0.4}F_3$ is FE with a polar COII pattern (although this has yet to be confirmed experimentally). Furthermore, the polar CO patterns induce "unbalanced" (from the valence point of view) planes at $z = 1/4$ and at $z = 3/4$, so that a monoclinic crystal distortion is expected (in this case along the direction of P, determined by the COII pattern as well). This is proposed as responsible for the reported FEL phase [9]. To check this effect, we optimized the a, b, c lattice vectors under COI and COII patterns, keeping the cell volume fixed to the experimental value. It

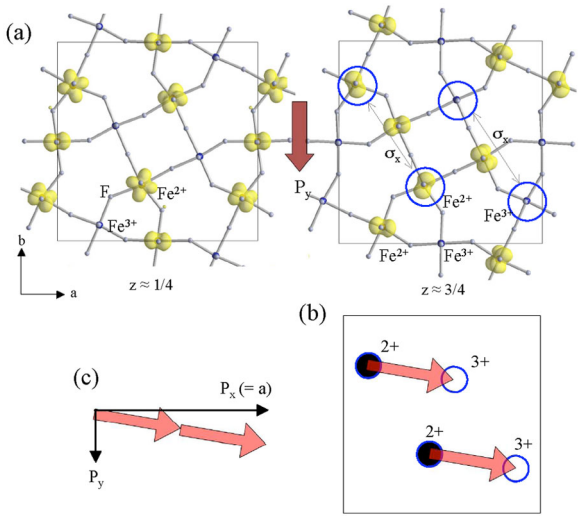

FIG. 3 (color online). (a) Down-spin charge of Fe t_{2g} states, within an energy range up to 1 eV below E_F, in the optimized structure with the COII-σ_x pattern. Circles show the Fe sites where $Fe^{2.5+}$ mixed-valence ions are originally located in the experimental structure. (b) Electric dipoles arising among circled Fe sites, due to the different valence occurring upon full CO. (c) The polarization P_x has the same size as the a Bravais vector with one electron charge (2π in Berry phase), so that P_x is zero; on the other hand, the net P_y is nonzero.

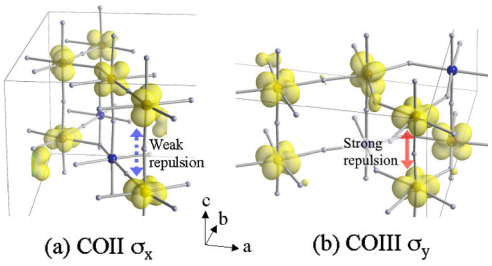

FIG. 4 (color online). Perspective view of OO of Fe-t_{2g} down-spin states [same energy range as in Fig. 3] at (a) COII and (b) COIII. The strong or weak next-neighbor orbital overlap and the consequent intersite Coulomb repulsion is highlighted.

turns out that the optimized lattice is in fact monoclinically distorted, with an angle $\angle bc = 90 - 0.059°$ at COII, and an $\angle ac = 90 - 0.040°$ at COIII. Significantly, FEL is strongly coupled with CO, which in turn determines the direction of the FE polarization. The FEL distortion in the ac or bc plane is peculiar to this CO system and distinct from the conventional monoclinic distortion in the ab plane, the latter occurring in other FEL TTB compounds, e.g., BNN, as well. Although these monoclinic distortions in $K_{0.6}Fe^{II}_{0.6}Fe^{III}_{0.4}F_3$ were not experimentally observed, we remark that they are rather small and possibly below the detection limit.

Ferroelectric anisotropy.—The proposed polar COII pattern may not be spontaneously long ranged; however, it may be possible to stabilize large FE domains by field cooling upon applying E_y, in analogy with $LuFe_2O_4$ (where the FE and the anti-FE states are energetically close and the stabilization of the FE phase occurs via field cooling). We further speculate that the energetically competing COIII pattern inducing a large P_x might be realized by applying E_x. In the case of a (strong enough) applied electric field rotating in the xy plane, the induced P along the field would therefore change its saturation value. This ''ferroelectric anisotropy'' (FEA), denoted as the energy required to modify the direction (as well as size) of the permanent polarization by switching the crystal between different CO phases (in this case COII and COIII), may find applications in future devices, such as multiple-state memories where the information can be stored by exploiting not only the sign of P, but also its direction. The FEA is peculiar for ''improper'' ferroelectricity induced by electronic degrees of freedom; in analogy with CO-induced polarization, the possibility to control the direction of **P** in spin-spirals manganites by means of a magnetic field was already proven and suggestions towards devices harnessing FEA already came [26].

In summary, tungsten-bronze systems, previously known for hybridization-driven d^0 ferroelectricity occurring in BNN, branch into the class of improper multiferroics. Indeed, we have put forward CO as the origin of ferroelectricity (as well as of some FEL modes) in a non-oxide TTB compound, $K_{0.6}Fe^{II}_{0.6}Fe^{III}_{0.4}F_3$. Several energetically competing CO patterns were predicted from first principles, with potentially different directions and magnitudes of the polarization. This ''ferroelectric anisotropy,'' typical of electronic magnetic ferroelectrics, shows a high technological appeal in multiple-state devices. In addition, the strong interplay between CO, ferroelasticity, and ferroelectricity in $K_{0.6}Fe^{II}_{0.6}Fe^{III}_{0.4}F_3$ makes it an excellent compound where multiferroic effects are manifestedly at play.

We thank F. Mezzadri, E. Gilioli, and G. Calestani for useful discussions. The research leading to these results has received funding from the European Research Council under the EU 7th Framework Programme (FP7/2007-2013)/ERC Grant Agreement No. 203523. Computational support from Caspur Supercomputing Center (Rome) is acknowledged.

[1] S. Picozzi and C. Ederer, J. Phys. Condens. Matter **21**, 303201 (2009).
[2] M. Mostovoy and S. W. Cheong, Nature Mater. **6**, 13 (2007).
[3] T. Kimura *et al.*, Nature (London) **426**, 55 (2003).
[4] D. V. Efremov, J. van der Brink, and D. I. Khomskii, Nature Mater. **3**, 853 (2004).
[5] S. Picozzi *et al.*, Phys. Rev. Lett. **99**, 227201 (2007).
[6] N. Ikeda *et al.*, Nature (London) **436**, 1136 (2005).
[7] M. Alexe *et al.*, Adv. Mater. **21**, 4452 (2009).
[8] K. Yamauchi, T. Fukushima, and S. Picozzi, Phys. Rev. B **79**, 212404 (2009).
[9] F. Mezzadri *et al.*, Phys. Rev. B **78**, 064111 (2008).
[10] P. B. Jamieson, S. C. Abrahms, and J. L. Bernstein, J. Chem. Phys. **48**, 5048 (1968).
[11] J. F. Scott, J. Phys. Condens. Matter **20**, 021001 (2008).
[12] G. Kresse and J. Furthmüller, Phys. Rev. B **54**, 11169 (1996).
[13] P. E. Blöchl, Phys. Rev. B **50**, 17953 (1994).
[14] V. I. Anisimov, F. Aryasetiawan, and A. I. Lichtenstein, J. Phys. Condens. Matter **9**, 767 (1997).
[15] R. L. Barns, J. Appl. Crystallogr. **1**, 290 (1968).
[16] R. D. King-Smith and D. Vanderbilt, Phys. Rev. B **47**, 1651 (1993).
[17] H. J. Xiang and M.-H. Whangbo, Phys. Rev. Lett. **98**, 246403 (2007).
[18] J. Burgeat and J. C. Toledano, Solid State Commun. **20**, 281 (1976).
[19] J. C. Toledano, Phys. Rev. B **12**, 943 (1975).
[20] N. A. Hill, J. Phys. Chem. B **104**, 6694 (2000).
[21] K. Sambasiva Rao and K. Hyun Yoon, J. Mater. Sci. **38**, 391 (2003).
[22] J. Ravez, S. C. Abrahams, and R. de Pape, J. Appl. Phys. **65**, 3987 (1989).
[23] Y. Calage *et al.*, J. Appl. Phys. **67**, 430 (1990).
[24] S. Fabbrici *et al.*, Chem. Mater. **16**, 3007 (2004).
[25] See supplementary material at http://link.aps.org/supplemental/10.1103/PhysRevLett.105.107202.
[26] E. Schierle *et al.*, arXiv:0910.5663.